An Evaluation of an Ultra-High Frequency Electromagnetic Fields Energy and Recovery Solutions

Aurel CHIRAP, Eugen COCA, Dan Alin POTORAC
Department of Computers, Electronics and Automation
Stefan cel Mare University of Suceava, Romania
aurel@eed.usv.ro, eugen.coca@usv.ro, alinp@eed.usv.ro

***Abstract*—The unprecedented development of wireless communications has led to a steady increase in the number of electromagnetic field generators. Thus, the environment has reached an unseen network of electromagnetic energy-carrying waves. In this paper, we present the results of a study to estimate the EMF-UHF propagation attenuation from the outside environment to the interior, to see if it is possible to place flat antennas on a glazed surface in order to capture and recover EMF energy. Furthermore, a stand composed of two groups of rectifier antennas whose performance was evaluated under real ambient / external environment conditions has been built. Thus, it was possible to experimentally verify the concepts of energy harvesting and energy scavenging, the capture and recovery of micro-energy produced by the presence of EMF-UHF with low power density in the environment.**

Keywords—Energy harvesting, Energy scavenging, Rectenna, Electromagnetic field, Renewable energy sources, Micro energy, Attenuation measurement.

I. INTRODUCTION

The accelerated development of wireless communications technologies determined an increasing number of electromagnetic field generating sources, mostly affecting the urban environment. There are regulations on the power emissions of fixed or mobile equipment used in wireless communications [1]. There are also regulations on exposure limit values for electromagnetic fields [2-3]. Therefore, the ultra high frequency electromagnetic field (UHF-EMF) strength in the ambient environment is expected to be lower or at least equal to the regulated values.

Wireless charging solutions already available on the market are specifically designed to generate a powerful and concentrated RF. The principle of transferring ultra-high-frequency wireless power was first experienced in the late 1950s [4-5].

Considering the last years massive expansion of wireless communications, RF fields are present today everywhere so it has become a challenge to develop RF energy recovery solutions without building dedicated generators, just by "scavenging" the existing RF surroundings. The concept of "RF power scavenging" has a relatively recent history that occurs in the context of the accelerated development of mobile communications networks [6-9]. Even though the incident wave power level is very low, DC energy resulting from conversion can be accumulated for extended periods of time in capacitors or batteries [10]. Accumulated energy can be used to support the short-term peaks in energy consumption specific sensor nodes.

In order to identify the best EMF capture opportunities available in the some transmitters' coverage areas, it is necessary to know the emission frequencies, the emission power or average power at the coverage limit, the type of carrier frequency polarization, information that is not always publicly accessible. For the sake of clarity, reference may be made to the "National Radio Frequency Allocation Table" [3], however this does not provide us with information on the physical magnitudes that characterize EMF.

There is a wide range of sources emitting high frequency electromagnetic fields. All of them are differentiated by specific parameters such as the emission power, the frequency emission band and the location. We propose for this study two scenarios of spectral analysis: for indoor and for the external environment.

The novelty of the researches described in this article is related to the identification, design and test practical solutions for use the energy offered by the weak RF communications fields.

II. MEASUREMENT AREA

The study location selection, a building on the campus of the university, was determined by two aspects. Firstly, this location is covered by a local WiFi network [11], see Fig. 1. Secondly, because on a wide area [12] around this location there are several potentially generating EMF sources, located at different distances, from 154m (S4) to 705m (S1), as can be seen in Fig. 2.

978-1-5386-1495-2/18/$31.00 ©2018 IEEE

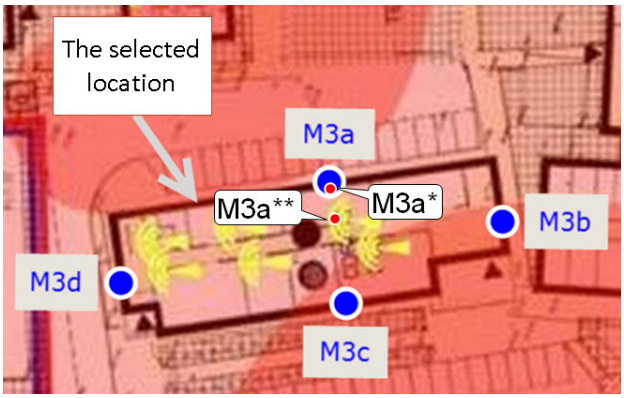

Fig. 1. Local WiFi network coverage and several sampling points.

Starting from the assumption that S1-S4 are EMF generating sources with unknown technical parameters, it is necessary to identify a method by which information about the electromagnetic field existing in the distant area of these sources can be obtained. This case considered is one of the campus buildings, C FIESC. The EMF power density at some point in the transmitter distant field is dependent on its parameters, the distance to that point and the propagation medium characteristic impedance. The free space characteristic impedance is:

$$\eta_0 = \sqrt{\mu_0 / \varepsilon_0} = 120\pi = 377\Omega \quad (1)$$

where: μ_0 is the permeability, and ε_0 is the permittivity of the free space.

At some point in the far field a power density estimate can be done by applying the relation:

$$S = P_t G_t / 4\pi r^2 \quad (2)$$

where: S is power density in W/m, P_t is transmitted power in W, G_t is transmission gain, and r is distance in meters between the emission source and the point where reception is made.

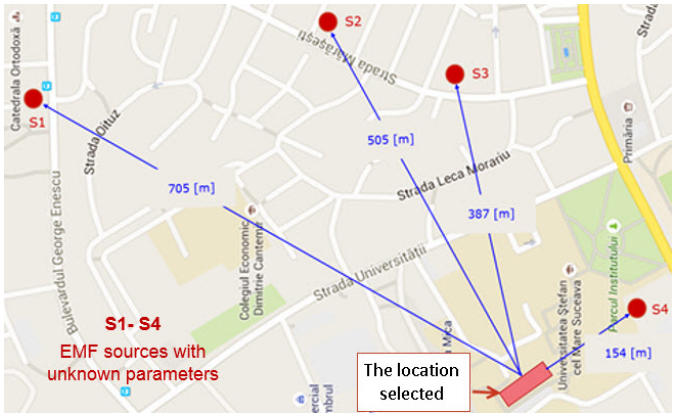

Fig. 2. Distributions and distances to which the EMF sources are located relative to the location where sampling was performed.

Equation (2) is also known as the Friss equation for far field. Since P_t and G_t are unknown, this equation can not be used to estimate the power density in the given case. In this context a possible solution for EMF characterization in the far field of the generating source is the specialized measuring equipment use.

As we know, the high frequency electromagnetic field is characterized by the magnetic component (H) as well as the electrical component (E). The physical magnitudes associated with the two components are: the magnetic induction field strength, expressed in A/m, respectively the electric field strength, expressed in V/m. By knowing the electrical field strength for high frequency, we can calculate the power density expressed in W/m2, applying the equation:

$$S = \eta_0 |H|^2 = |E|^2 / \eta_0 \quad (3)$$

III. Measurement Setup - Equipment and Method.

To estimate the EMF strength, a particular sampling method was used on four different points M3a → M3d, as represented in Fig. 1. The measurement system used for sampling is shown in Fig. 3 and consists of equipment and devices.

1) Spectrum analyzer - Anritsu MS2724B [13];

2) Receiver antenna - 489-DB broadband log-periodic antenna [14];

3) Coaxial cable - type SUCOFLEX-104P [15], impedance 50 Ω, maximum operating frequency 26.5 GHz;

4) Telescopic tripod - maximum height 3 m used to fix the antenna;

5) Desktop System - used for sample processing.

Sampling has been made both in the outside environment as well as indoors. The method used for sampling involved two stages. First step was to obtain an overview of the existence of EMF in the outdoor environment. Thus, a set of samples was drawn from which the spectral diagrams and maximum EMF values were extracted during a 6 minutes time interval (Fig. 4).

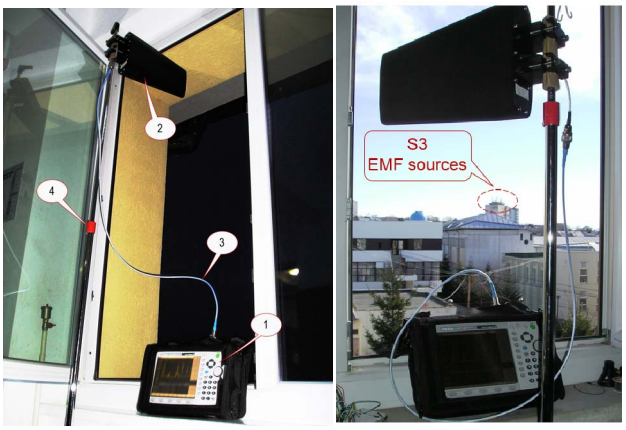

Fig. 3. Configuration of the measurement system used for sampling.

Preliminary recordings highlighted the frequency bands that occupy parts of the spectrum analyzed as well as the EMF power in each band.

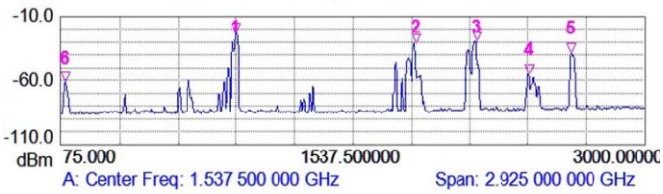

Mkr	Ref	Delta	Ref Freq	Ref Amp	Delta Freq	Delta Amp
1	■	□	952.500 000 MHz	-22.38 dBm	- -	- -
2	■	□	1.856 590 909 GHz	-30.63 dBm	- -	- -
3	■	□	2.159 727 273 GHz	-29.00 dBm	- -	- -
4	■	□	2.425 636 364 GHz	-54.44 dBm	- -	- -
5	■	□	2.633 045 455 GHz	-37.93 dBm	- -	- -
6	■	□	96.272 727 MHz	-60.81 dBm	- -	- -

Fig. 4. Spectral diagram of the 75 MHz - 3 GHz frequency range the peak EMF values recorded over 6 minutes at the M3a sampling point.

As can be seen in the spectral diagram in Fig. 4 the EMF power is extremely low over the frequency range 75 MHz to 800 MHz, therefore this interval will be excluded from the next sampling phase.

In the second step, for each sampling point two field strength measurements were made, one to obtain peak value and the other to determine the maximum RMS value (square root of the square of the strength squares) for periods of six minutes.

Moreover, at the sampling point M3a three sets of measurements were performed. Two sets of measurements aimed at estimating the power density on the outside and the inner part of the separation medium, in this case the thermopan glass made window, to see the degree of attenuation of EMF propagation. The third set of measurements aimed at assessing the EMF power density indoor, in which case the receiving antenna was placed at a distance of 4.6m from the outside plane of the windows, in this case the glass being only part of the separation medium with the exterior. The following section selectively highlights part of the results obtained from sample processing.

IV. Results and Discussion

The preliminary measurements results, performed at the four sampling points, highlighted in Fig. 1, are presented in a synthetic form in Fig. 5 diagram. Analyzing the diagram it can be seen that the maximum values of EMF are predominant in the 900 MHz and 2100 MHz frequency bands, the highest value was recorded at the M3b sampling point. It should be noted that at the sampling point M3c, the minimum EMF values for the external sources frequency bands were recorded.

The minimum values are explained by the fact the M3c sampling point with no direct visibility to the external EMF sources is due to track losses due to the structure of the building. It can also be observed that EMF levels with close values were recorded at the M3a and M3d sampling points, the maximum recorded in the 900 MHz band and the minimum bandwidth of 2600 MHz.

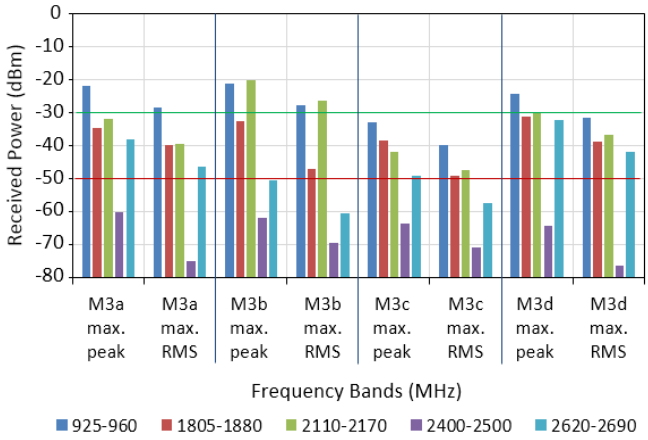

Fig. 5. Comparative representation of EMF power (in dBm), measured in the external environment at the sampling points M3a-M3d.

The measured field strengths at the sampling point M3a for the EMF reception in three different cases are presented in the tables in which the power densities calculated with the relation (3).The field strength measured at the sampling point M3a and the power density calculated for EMF reception in the three cases described in Section III are shown in the Table I, Table II and Table III.

TABLE I. Field Strength and Power Density for the External Environment and Sampling Point M3A (*)

Frequency band (MHz)	Field strength (V/m) (1)		Power density (μW/m²) (2)	
	max. peak	max. RMS	max. peak	max. RMS
925-960	0.547	0.255	794.079	172.572
1805-1880	0.390	0.161	403.662	68.792
2110-2170	0.650	0.179	1121.285	85.035
2400-2500	0.070	0.018	13.004	0.841
2620-2690	0.260	0.071	179.406	13.530
□*□ - the receiving antenna positioned at 1.55 m height perpendicular to the plane of the separation medium outside it.				
□¹□ - measured values; □²□ - calculated values.				

TABLE II. Field Strength and Power Density for the Indoor and Sampling Point M3A (*)

Frequency band (MHz)	Field strength (V/m) (1)		Power density (μW/m²) (2)	
	max. peak	max. RMS	max. peak	max. RMS
925-960	0.0409	0.0170	4.440	0.767
1805-1880	0.0610	0.0307	9.875	2.501
2110-2170	0.0304	0.0158	2.453	0.662
2400-2500	0.0546	0.0111	7.912	0.327
2620-2690	0.0163	0.0040	0.705	0.042
□*□ - the receiver antenna positioned at 1.55 m height perpendicular to the inner plane of the separation medium in the immediate vicinity of it.				
□¹□ - measured values; □²□ - calculated values.				

TABLE III. FIELD STRENGTH AND POWER DENSITY FOR THE INDOOR ENVIRONMENT AND SAMPLING POINT M3A (**)

Frequency band (MHz)	Field strength (V/m) [1]		Power density (μW/m²) [2]	
	max. peak	max. RMS	max. peak	max. RMS
925-960	0.1293	0.0715	44.370	13.568
1805-1880	0.0686	0.0370	12.489	3.633
2110-2170	0.0871	0.0495	20.134	6.503
2400-2500	0.1161	0.0178	35.773	0.841
2620-2690	0.0271	0.0089	1.949	0.210
□*□ - the receiver antenna is positioned at 1.55 m height and the 4.6 m distance of perpendicular to the inner plane of the separation medium.				
□[1]□ - measured values, □[2]□ - calculated values.				

EMF attenuation under conditions where different electromagnetic waves of different frequencies, emitted from external sources, cross a separation medium such as the insulating glass is highlighted in Table IV.

TABLE IV. THE LEVEL OF EMF ATTENUATION IN THE INDOOR ENVIRONMENT.

Frequency band (MHz)	M3a(*) max. peak	M3a(**) max. peak
925-960	13.37	4.23
1805-1880	6.39	5.69
2110-2170	21.38	7.46
2400-2500	1.28	0.60
2620-2690	15.95	9.59

V. RECTIFYING ANTENNA - DESCRIPTION AND EVALUATION.

The results of the case study presented in Section IV highlighted that the EMF propagation attenuation through the glazed surface is the lowest in the GSM-1800 band (see Table IV). As a consequence, the power density at the inside of the glazed surface is the highest, 2.5μW / m2, which would recommend the use of some antennas made in planar technology. This is the reason why an experiment is proposed to capture, convert and recover the micro-energy available in the GSM-1800 frequency band. A rectifier antenna for this purpose is generically represented in Fig. 6.

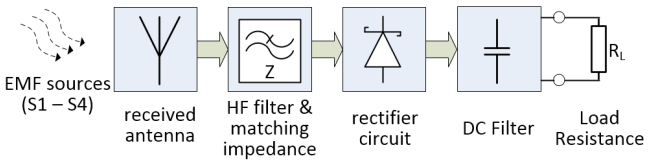

Fig. 6. Rectenna - generic representation.

A. Receiving antenna

In order to capture the micro-energy from the ambient environment, the coplanar broadband monopoly antenna was proposed whose geometry is shown in Fig. 7. The antenna dimensioning was done according to the method described in [16] and adapted to the requirements of the present case. The simulation was done in ADS and the prototype antenna was made on FR4 laminate with 1.5mm substrate thickness.

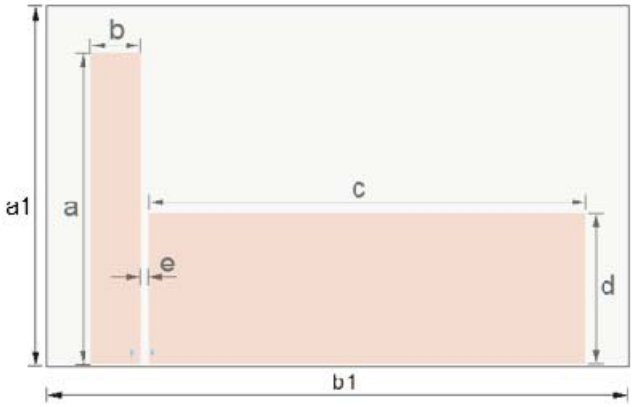

	a	b	c	d	e	a1	b1
(mm)	43.6	7.0	61.3	21.2	1.0	50.5	81.5

Fig. 7. Geometry descriptors for the proposed antenna.

The qualitative assessment of the prototype antenna was based on established and frequently used antenna ratings. Thus, in the graphical representation from Fig. 8, a good similarity can be observed between the evolutions of the measured return losses as compared to the simulation results. It is also noted that bandwidth BW = 2.45 GHz is delineated by fL and fH markers for a return loss level of - 9.54 dB, in which case the stationary wave rate SWR is 2: 1. Ideally, the antenna should have SWR = 1, in which case the input reflection coefficient and the reactive component will have a null value, meaning that all the power captured by the antenna is transferred to the load.

However, the simulation results as well as those obtained by measurement indicate that a SWR close to the unit is only possible around the resonance frequency. Often, in practice, more important is the bandwidth than the goal of getting unitary SWR. If an antenna is going to have a wider bandwidths, then an increase in the SWR should be accepted, in which case the consequence is the decrease the captured power.

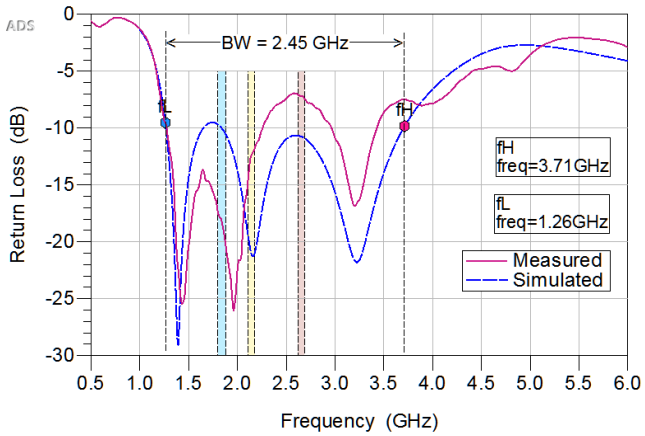

Fig. 8. The measured and simulated Return Loss (S11) of the proposed antenna.

B. Rectifier circuit

The efficiency of an ultra-high frequency rectifier circuit depends in a large extent on the chosen Schottky diode type and on circuit configuration, but is also related with the network impedance matching level. Schottky silicon diodes are distinguished by their barrier capacity that depends on the type of metal used in forming the metal-semiconductor junction. The barrier capacity may be low, medium or high, and this dictate the switching speed between conduction and locked state. Thus the switching time may vary from a few picoseconds to tens of picoseconds.

In general, the opening voltage of a Schottky Silicon diode is 300mV. There is a special category of Schottky diodes (Zero Bias Detector) that do not require polarization from an external voltage source and have a 150 mV open voltage. Therefore, we consider that these are most suitable for the recovery of ultra-high frequency signals and ultra-low power capture. Thus, two types of Schottky diodes with different encapsulations were selected: SMS7630-097LF (SOD-523 capsule) [17] and HSMS-286C (SOT-323 capsule) [18].

After creating the linear model of the selected diode, having as reference the data sheet parameters, different configurations of the rectifier circuits were simulated and evaluated by the following steps:

a) Simulation of the linear model for impedance determination at the rectifier circuit input, as can be seen in Fig. 9, and dimensioning the impedance matching network at a standard input port.

b) Dynamic simulation of the rectifier circuit using the non-linear diode model, with monitoring of the DC voltage and current at the rectifier output, under the following conditions:

- Variable input power, from -40dBm to 10dBm;

- Variable load resistance, from 100 Ohm to 100 kOhm;

- Variable frequency, considering the bandwidth edge frequencies and the center frequency of the band.

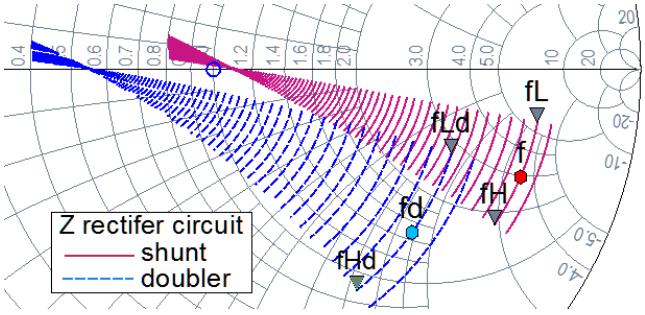

Frequency	doubler	shunt
fL; fLd (900 MHz)	138.43 -j83.67	276.87 -j167.35
fL; fd (1840 MHz)	73.86 -j88.65	147.73 -j176.33
fH; fHd (2700 MHz)	43.86 -j72.85	87.733 -j145.70

Fig. 9. Impedance variation with the frequency of rectifier circuits with SMS7630-079LF diodes, shunt and duplex configurations.

Following the evaluation of the simulated rectifier circuits in the ADS environment, it was observed that for input power below -30 dBm, the voltage at the terminals of the load resistor is slightly increased in the case of the shunt configuration as compared to the doubled voltage circuit. This aspect is comparatively highlighted in the diagram from Fig. 10 where the m1 and m2 markers are indicating the output voltage if RLoad = 10KΩ and the input power is -30dBm.

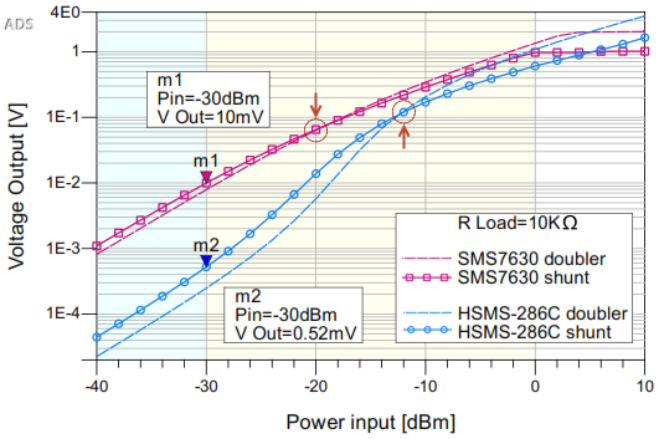

Fig. 10. The output voltage as a function of the input power.

Also on the diagram in Fig. 10 is indicated the input power from which the voltage doubling rectifier configuration becomes more efficient than the shunt configuration. The rectifier circuit with the SMS7630-079LF diode as shunt configuration was built on a RO4003C laminate (0.81mm substrate thickness, relative permittivity εr = 3.55, dielectric loss tanks = 0.0027) and measured to determine the efficiency of RF-DC conversion. Fig. 11 shows the efficiency of RF-DC conversion for four RF power steps depending on a load whose value varies from 100 Ohm to 30 Kohm.

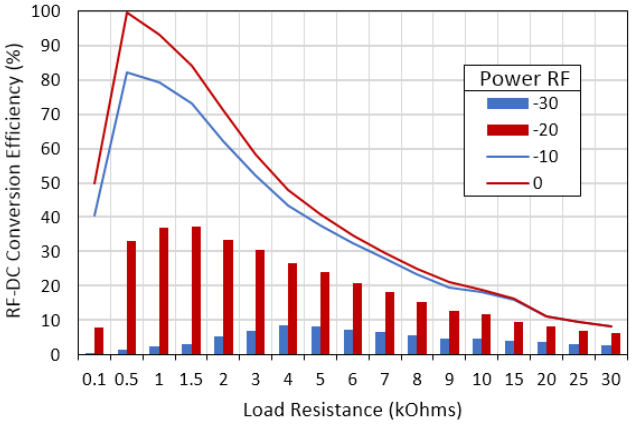

Fig. 11. The measured RF-DC conversion efficiency of the rectifier M3 versus load resistance for the input power level from -30 dBm to 0 dBm.

VI. Experimental Validation of the Theoretical Concept

Based on the results of the evaluation of the antenna and the rectifier circuit summary presented in Section V, a stand

was developed (see Figure 12) to allow a real life evaluation of the ultra-high frequency electromagnetic field capture and its energy conversion taken from environmental existing ultra-high frequency electromagnetic field.

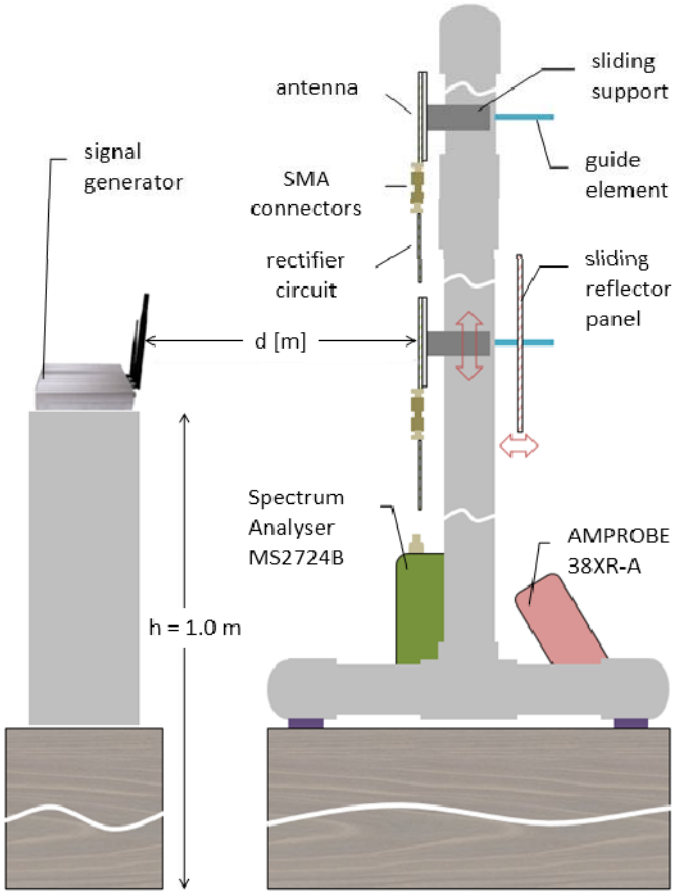

Fig. 12. Schematic representation of the stand and configuration used in a test scenario.

The experimental stand is composed from two groups of five rectifier antennas mounted on a sliding support provided with two guiding elements to support a single-sided FR4 panel and used as a reflector. The fact that the reflector panel slides over the guide elements allows positioning at a certain distance from the receiving antennas. Three different scenarios, described below, were used to perform the measurements, as below.

A. Energy harvesting using wireless power transfer

In this scenario, deployed in a laboratory environment, the transfer of wireless power from a signal generator to the R1, R3, R5 rectifier antennas is demonstrated. The location of the equipment used in the experiment is shown in Fig. 12. In the histograms of Fig. 13 we compare the voltage variation at the RLoad resistor terminals as a function of the received RF power, without a reflector panel and with a reflector panel positioned at a distance of 4.7 cm from the receiving antennas.

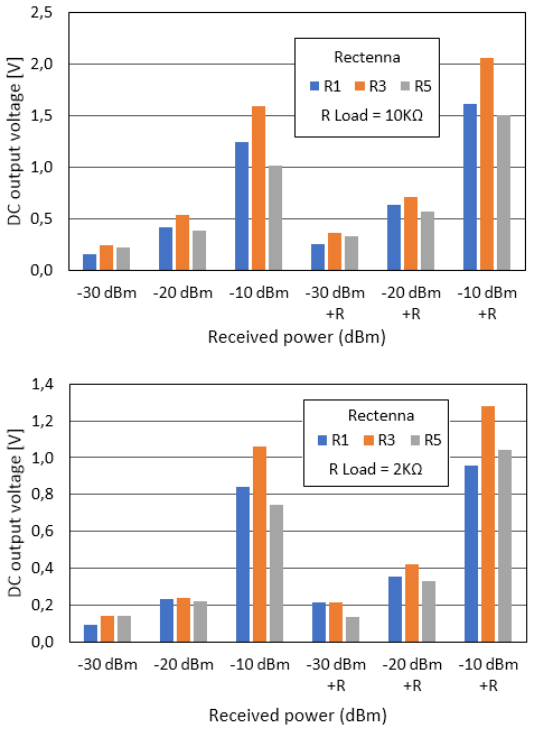

Fig. 13. The rectennas R1, R3, R5, output voltage on RLoad = 10Kohms, respectively 2 Kohms corresponding to a reception of powers -30 dBm, -20 dBm, -10dBm.

Table V gives the power available at reception, measured with the MS2724B spectrum analyzer, as a function of the distance between the transmitter and the proposed receiver antenna.

TABLE V. THE POWER AVAILABLE AR THE RECEPTION AS A FUNCTION OF THE DISTANCE

Received power	Distance (d)
-30 dBm	6 m
-20 dBm	3m
-10 dBm	1m

B. Energy scavenging in real environment

In this scenario, the rectifier antenna booth was placed in the sampling points M3a and M3a** (see Fig. 1) and the DC voltage has been measured for two different values of R_{Load}, 10KΩ and 2KΩ load respectively, without and in the presence of the reflector panel.

Samples are the peak voltages recorded over 6 min time intervals. Sampling at point M3a (external environment) was done for two different situations. In the first situation the antennas are oriented to the S3 source assuming that the angle of incidence of the waves is 0^0. In the second situation, assuming that the incident angle of the waves is 30^0, the antennas were positioned in parallel with the glazed surface.

The histograms in Fig. 14, Fig. 15 and Fig.16 compares the voltage values provided by the R1, R3, R5 rectifier antennas to the R_{Load} resistor terminals for the two situations.

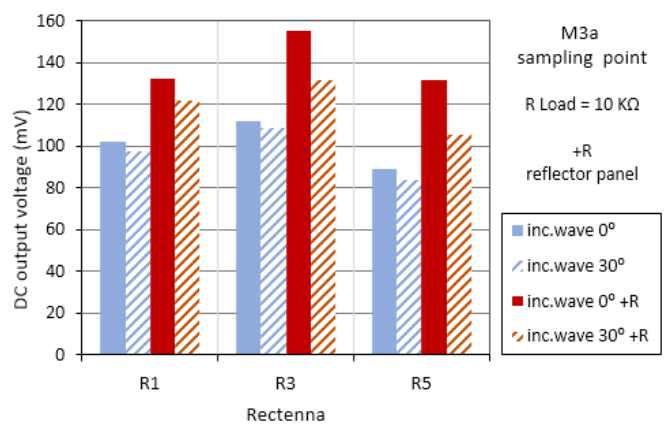

Fig. 14. Output voltage histogram for the rectifier antennas R1, R3, R5. Values measured at the sampling point M3a.

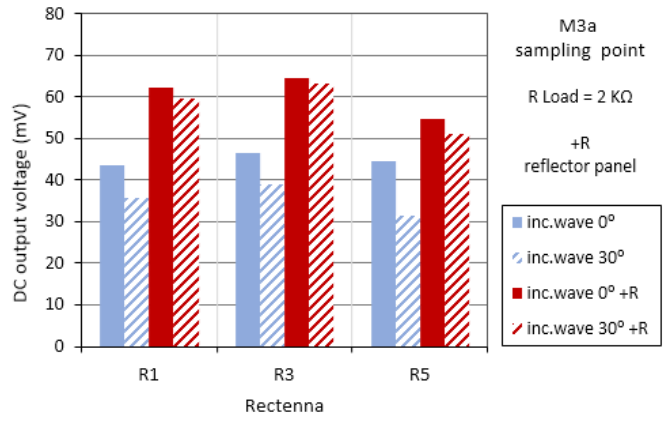

Fig. 15. Output voltage histogram for the rectifier antennas R1, R3, R5. Values measured at the sampling point M3a, for different antenna inclinations and 2 kohms load.

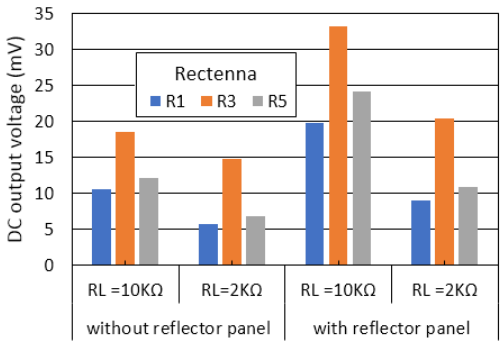

Fig. 16. Output voltage histogram for the rectifier antennas R1, R3, R5. Values measured at the sampling point M3a** for different loads.

C. Operations of the Sensor Node with the energy accumulated by the Wireless Power Transfer System

The board of the sensor node provides four sensors that can retrieve data from the environment for: light, temperature, humidity and motion. For data transmission, the IPS-EVAL-EH-02 incorporates the MiWi 2.4GHz IEEE Std. 802.15.4 RF transceiver module from Microchip [12].

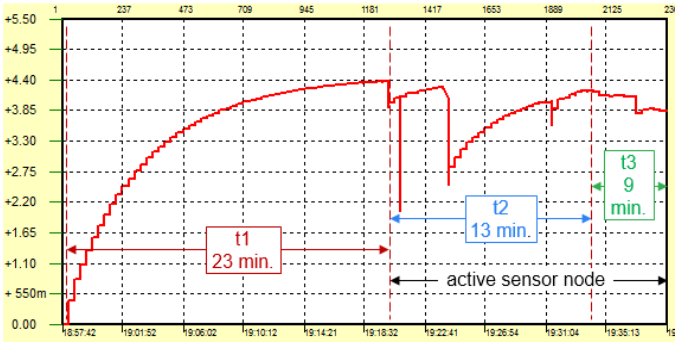

a)

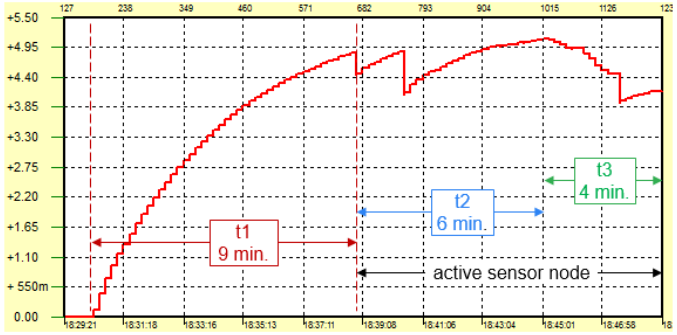

b)

Fig. 17. Variation of DC voltage at the supercapacitor terminals used as energy storage buffer for the energy recovered by R1, R3, R5 rectifier antennas, for a RF power transfer of -10dBm for a) without reflector and b) with a reflector panel positioned at 4.7 cm.

The scenario tracks the operation of the sensor node with the captured energy resulting from the received RF power transfer at a level of -10dBm. The power supplied by three rectifier antennas with serial outputs is accumulated in two energy buffers, a primary buffer consisting of two supercapacitors connected in parallel (2x100mF / 5.5V) and a secondary buffer that accumulates energy in a thin film battery MEC201-7S; 4V / 0.7mAh). Voltage monitoring at the primary buffer terminals allowed the determination of the time required for energy accumulation to enable the sensor node to operate. In the diagrams in Fig. 18 shows the voltage variation curves at the main buffer terminals for the two cases: rectifier antennas without / with reflector panel.

Marking the time periods on the diagrams in Fig. 16 has the following meanings:

• t1 - the time at which the RF source transmits and accumulates energy in the two buffers, the transition to time t2 is only performed if the condition of the secondary buffer reaches the 4.2 Volts moment at which the sensor node becomes active;

• t2 - the sensor node is active and at the same time the accumulation of energy transmitted from the RF source takes place.

• t3 - the time at which the sensor node is active and only works with the energy accumulated in the two buffers.

In Fig. 18 it is presented the stand with the rectifier antennas and the sensor node used for the experiment.

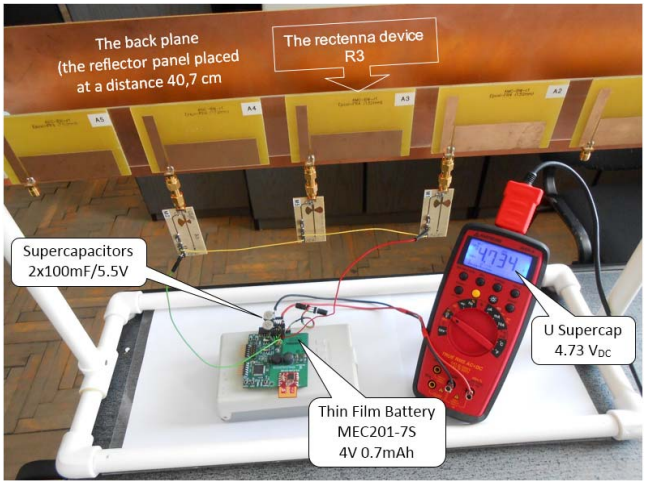

Fig. 18. Rectifying antennas and the active sensor node.

VII. CONCLUSION

Experimental results validate the theoretical concepts underpinning the energy recovery from wireless power transfer and micro energy recovery from the ambient environment in which the ultra high frequency and ultra low power electromagnetic fields are present.

ACKNOWLEDGMENT

This paper has been supported by the research plan of Ministry of National Education from Romania. The authors also acknowledge the technical support from Keysight Technologies and Rogers Corporation.

REFERENCES

[1] „ETSI - European Telecommunications Standards Institute". [Online]. Available at: http://www.etsi.org/.

[2] The Council of the European Union, „Recommendation on the limitation of exposure of the general public to electromagnetic fields (0 Hz to 300 GHz)". Official Journal of the European Communities, 12-iul-1999.

[3] MCSI- The Ministry of communications and information technology and ANCOM - National Authority for Management and Regulation in Communications, „Table of allocation of radio frequency bands". oct-2011.

[4] W. C. Brown, „The History of Power Transmission by Radio Waves", IEEE Transactions on Microwave Theory and Techniques, vol. 32, nr. 9, pp. 1230-1242, sep. 1984.

[5] W. Brown, J. Mims, and N. Heenan, „An experimental microwave-powered helicopter", vol. 13, pp. 225-235.

[6] H. J. Visser, A. C. F. Reniers, J. A. C. Theeuwes, „Ambient RF Energy Scavenging: GSM and WLAN Power Density Measurements", 2008, pp. 721-724.

[7] S. Keyrouz, H. J. Visser, and A. G. Tijhuis, „Ambient RF energy harvesting from DTV stations", 2012, pp. 1-4.

[8] M. Pinuela, P. D. Mitcheson, and S. Lucyszyn, „Ambient RF Energy Harvesting in Urban and Semi-Urban Environments", IEEE Transactions on Microwave Theory and Techniques, vol. 61, nr. 7, pp. 2715-2726, iul. 2013.

[9] S. Kim et al., „Ambient RF Energy-Harvesting Technologies for Self-Sustainable Standalone Wireless Sensor Platforms", Proceedings of the IEEE, vol. 102, nr. 11, pp. 1649-1666, nov. 2014.

[10] W. C. Brown, „An experimental low power density rectenna", submitted to Microwave Symposium Digest, IEEE MTT-S International, Boston, MA, USA, 1991, pp. 197-200.

[11] DCTI-USV, „ A map of wireless equipment the Ştefan cel Mare University". [Online]. Available at: http://wireless.usv.ro/.

[12] Google Map Maker, „ A Map Of The Municipality Of Suceava". [Online]. Available at: http://goo.gl/YWo4nw.

[13] „Spectrum Master Handheld Spectrum Analyzer MS2724B - Anritsu Europe". [Online]. Available at: http://www.anritsu.com/en-GB/Products-Solutions/Products/MS2724B.aspx.

[14] Digital Antenna, „Wideband 800-2500 MHz Log Periodic Antenna - 10dB Gain". [Online]. Available at: http://www.digitalantenna.com/prods/cellantenna_wideband_logperiodic_10db.html.

[15] „Helmut Singer Elektronik - Gebrauchte und geprüfte Mess- und Kommunikationstechnik". [Online]. Available at: http://www.helmut-singer.de/php/suchliste.e.php.

[16] D. Laila, V. Deepu, R. Sujith, P. Mohanan, C. K. Anandan, şi K. Vasudevan, „Asymmetric Coplanar Strip fed wide band antenna", 2008, pp. 372-373.

[17] Skyworks Solution, Inc., „Surface Mount Mixer and Detector Schottky Diodes". 05-iul-2016.

[18] Avago Tehnologies, „HSMS-286x series. Surface Mount Microwave Schottky Detector Diodes". 26-aug-2009.

[19] D. Balan and A. Chirap, „Analysis of an eco-friendly sensor node powered by unconventional energy sources", 2014, pp. 1-4.